

A Review of Radio-Frequency Photocathode Electron Sources*

J. Stovall

MS H817, Los Alamos National Laboratory
Los Alamos, New Mexico 87545

Abstract

A review of this topic at the last conference in this series reported considerable progress in R&D programs aimed at producing high-current low-emittance electron beams using photocathode rf guns. At present at least 20 such projects are under way world wide and at least 6 photoinjectors are presently in operation. This paper reviews some of the choices that must be made in optimizing the design of the accelerating structure for a photoinjector based on the current state of knowledge.

A Historical Perspective

The first experimental results for a two-cell rf photocathode injector linac, or photoinjector, were reported by Los Alamos in 1988 [1]. This linac had two 1300-MHz rf cavities which were driven separately so that the phase and amplitude of each cavity could be controlled independently. The cathode was prepared on line in a special chamber and transferred under vacuum and seated on the front wall of the first cell. The multi-alkali cathode was illuminated by a laser having a wavelength of 532 nm. The performance of this injector is listed in Table 1.

TABLE 1
2-Cell Photoinjector Experimental Results

Parameter	Thermionic gun with buncher	Photoinjector
Q (nC)	5	15 (11)*
τ_{fwhm} (ps)	15	70
I (A)	300	200
ϵ_n (π mm mrad)	100	100 (40)*

* longitudinal tails deleted numerically

Q is defined as the total charge in one micropulse and τ is the length of temporal profile of the micropulse at the exit of the injector, measured at its full-width half-maximum point.

The peak beam current, $I = Q/\tau_{fwhm}$. The photoinjector community has recently adopted the convention of using the rms value for emittance, but for the purpose of this review the normalized emittance will be defined as

$$\epsilon_n = \beta\gamma\epsilon(90\%) = 4\epsilon_n(\text{rms}) \quad (1)$$

Table 1 also includes some typical values for a thermionic gun to which magnetic bunching has been added to achieve a beam of similar quality. While the beam

properties of this photoinjector did not eclipse the performance that could be expected from a more conventional gun, the results had some important implications. This experiment demonstrated that by tailoring the radial and temporal profile of the drive laser, the transverse and longitudinal shape and distribution of the electron beam could be modified. As a result, minimal beam loss in the accelerator can be assured.

In the case of a conventional gun the electron distribution within the microbunch is thermal. The beam distributions in transverse and longitudinal space from a photoinjector are correlated, which allows the important option of recovering emittance growth associated with space-charge effects. In addition, a series of experiments using the Los Alamos gun successfully verified that the design codes MASK, ISIS and PARMELA could be used with confidence in designing such devices and simulating their performance.

As a result of the pioneering work at Los Alamos there are now more than 20 experimental programs world wide to develop photoinjectors or photocathode linacs. Today there are six machines in operation, listed in Table 2 along with their operating frequencies. They span a factor of 20 in frequency and a factor of 10 in accelerating gradient. Presumably the design of each machine has been optimized for a specific application.

TABLE 2
Operating Photocathode Injectors

Institution	Frequency
BNL and CERN	2.85 GHz
Los Alamos: APEX and AFEL	1.3 GHz
Boeing Aerospace Corp. (BAC)	433 MHz
Bruyeres-le Chatel (CEA)	144 MHz

Applications

Two main applications have been identified which would not only benefit from photoinjector technology but in fact will probably require it. The first is a scheme for building a high energy (2 TeV) electron-positron linear collider. The concept, proposed by CERN, is a two-beam device in which a very high current drive beam is accelerated in a conventional linac at modest gradients. The power is extracted from the drive beam at 30 GHz to excite a very high gradient traveling-wave linac accelerating the collider beams, which have a more modest current. The beam parameters required for this scheme are listed in Table 3.

Free-electron lasers (FELs) also have requirements for very bright electron beams which are also listed in Table 3. Each micropulse must be short to maximize the peak current but long enough that it does not slip out of phase with the light packet it is driving. The geometric emittance must be

*Work supported by Los Alamos National Laboratory Program Development, under the auspices of the United States Department of Energy.

TABLE 3
Photoinjector Beam Requirements
Linear Collider FELs

Parameter	Drive beam	Collider beam	FELs
Q (nC)	64	1	5-10
τ fwhm (ps)	3	1	$\geq \tau_{\text{FEL}}$
I (kA)	20	1	> 0.1
ϵ_n (π mm rad)	-	1	$< \beta\gamma\lambda_{\text{FEL}}$

on the order of the FEL wavelength to assure good geometrical overlap between the FEL beam and the electron beam for efficient energy transfer. The FEL wavelength, λ_{FEL} , is a function of the wiggler magnet design and the electron beam energy. A part of this parameter space is shown in Fig. 1 along with the design operating points of several projects.

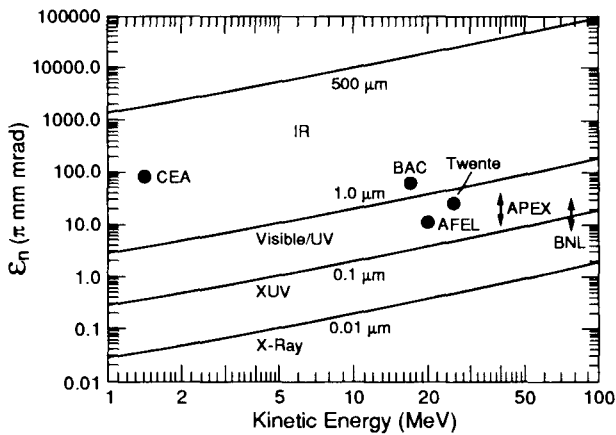


Fig. 1 Electron beam energy and emittance required in an FEL as a function of FEL wavelength.

Some Design Considerations

One of the unique features of high-gradient rf electron injectors is that the beam can be accelerated to relativistic energies in only one or two cells. In a typical FEL application the beam will spend about 50% of its lifetime in the first two cells of the machine. This probably accounts for the fact that most experimental photoinjector projects use a two-cell structure. The dominant effects that influence the beam quality, in addition to acceleration, are rf and space-charge forces.

In designing a photoinjector for either of the above applications one must remember that it is but one component of a larger complex machine including an accelerator, a transport system, and either wiggler magnets or energy extraction cavities. The beam correlations produced in the injector extend throughout the machine. The injector must therefore be considered as a part of an integrated design problem.

The electric field distribution in the first cell of a typical photoinjector is similar to that in the Los Alamos Advanced FEL (AFEL), which is plotted in Fig. 2. The radial component of the field, E_r , is typically linearized to reduce the nonrecoverable emittance growth that would otherwise

result from nonlinear rf defocusing. This has been achieved in the AFEL design by tailoring the contour of the exit aperture nose to match the lowest-order space harmonic of the field.

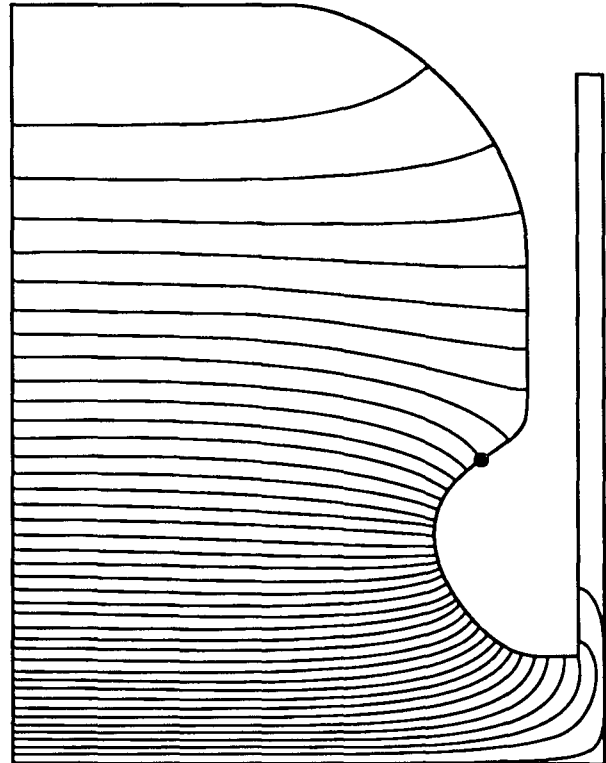


Fig. 2 Electric field distribution in the first cell of AFEL.

Competing requirements are maximizing both the shunt impedance and the accelerating field, E_{max} , while keeping the peak surface field, E_p , below the sparking limit. RF focusing can be added to the cavity by contouring the front wall of the cell adjacent to the cathode itself. The field can be shaped in this way so that electrons enter a converging electric field as they evolve from the cathode. This has been tested experimentally and the resulting focusing effect follows the prediction of the design codes. It has been shown however, that when constrained by a practical peak surface field limit, the field energy is better spent on rapid acceleration to relativistic energies than on focusing at low energy.

The axial component of the electric field, E_z , is plotted in Fig. 3. The cathode is typically illuminated at an injection phase of 22.5° . Electrons leaving late therefore see higher initial fields than those leaving early. The result is that the tail of the bunch gets shoved into the bunch, helping to overcome bunch lengthening due to space-charge forces.

The force due to the magnetic component of the rf field is, on the average, equal in magnitude to the radial force due to the electric field. Figure 4 shows the radial Lorentz force experienced by an electron at a distance of 3 mm from the axis.

$$F_r(\text{Lorentz}) = e(E_r + v \cdot B_\theta) \tag{2}$$

where e is the electronic charge, v is the velocity of the electron, and B_θ is the azimuthal component of the rf magnetic field. The parameter plotted is an equivalent electric field corresponding to the Lorentz force.

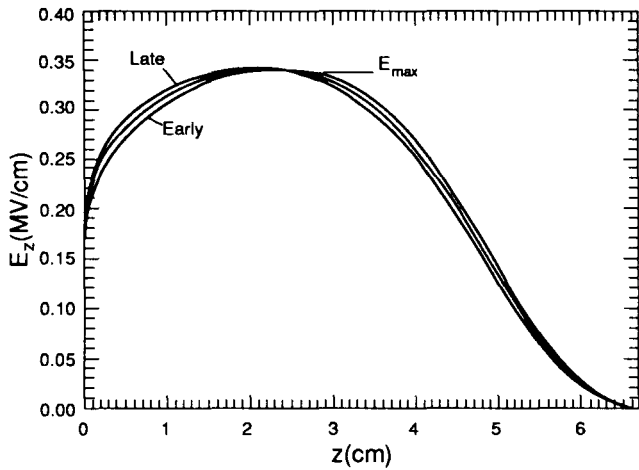


Fig. 3 E_z in cell one of AFEL.

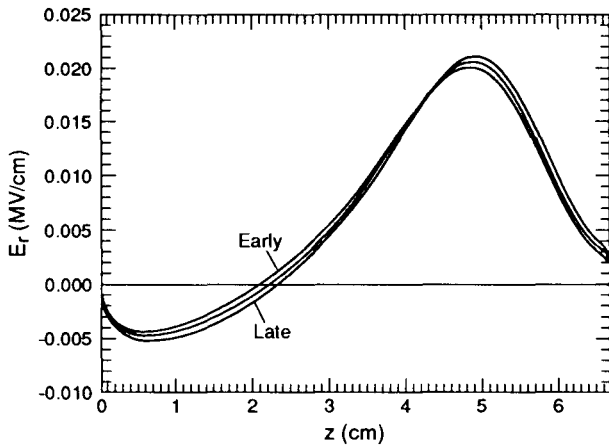


Fig. 4 Lorentz force equivalent field in cell one of AFEL.

As electrons leave the cathode, they experience a small focusing force from the magnetic field. This is followed by a large defocusing force from the combined electric and magnetic fields as the electrons enter the exit fringe of the cavity and the magnetic field has reversed. In all subsequent cavities where the relativistic velocity $\beta=1$, the Lorentz force integrates to zero.

Electrons leaving the cathode late see greater integrated defocusing forces than electrons leaving early. This causes a time-correlated "bow-tie" effect in transverse phase space that is very difficult to recover. Two schemes have been proposed, one involving higher harmonics in the cavity [2] and another requiring a separate independently phased cavity [3]. To date neither technique has been tested experimentally.

As noted above, electrons spend about half their lifetime in these fields. Figure 5 shows the axial electrical field in the time frame of the electron being accelerated as it passes

through the 11-cell AFEL linac. The beam is accelerated from rest to 20 MeV in only 400 ps. At 200 ps into their trip, however, the electrons have not emerged from the second cavity. Figure 6 shows the corresponding Lorentz force in the same time frame.

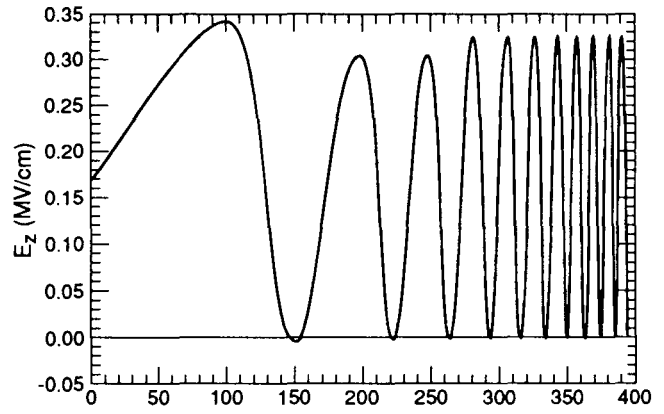


Fig. 5 E_z vs. time in the electron rest frame of AFEL.

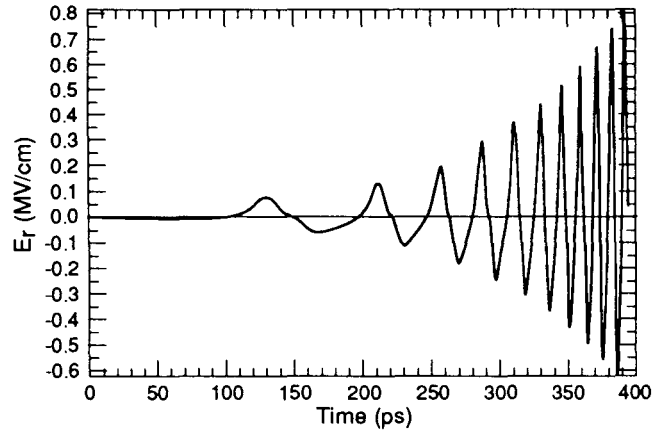


Fig. 6 Lorentz force equivalent field vs. time in the electron rest frame of AFEL.

A Theoretical Framework

An analytical model developed by Kim [4] helps give some insight into the relationship of some of the design parameters in a photoinjector. Making certain assumptions, the model derives separate expressions for emittance growth due to rf field effects and to space-charge effects. The rf electric field is assumed to be linear in r , the microbunch density distribution is assumed to be Gaussian in radius and length, the beam is allowed to increase unconstrained by any external restoring force, and the beam size is approximated by constant values in radius and length. The model predicts the following emittance growth relations.

$$\epsilon_{rf} \propto E_{\max} f^2 \sigma_r^2 \sigma_t^2 \quad (3)$$

$$\epsilon_{sc} \propto Q / E_{max} (3\sigma_r + 1.5\sigma_t) \quad (4)$$

E_{max} is the peak accelerating gradient on axis, f is the cavity rf frequency, σ_r is the average rms beam radius, and σ_t is the average rms bunch length.

Equating ϵ_{rf} and ϵ_{sc} allows the optimum peak field corresponding to minimum emittance growth to be derived from the model.

$$\epsilon_{min} = \epsilon_{rf} = \epsilon_{sc} \quad (5)$$

$$\epsilon_{min} \propto \frac{\sqrt{Qf} \sigma_r \sigma_t}{\sqrt{(3\sigma_r + 1.5\sigma_t)}} \quad (6)$$

$$E_{max}(\text{optimum}) \propto \frac{\sqrt{Q}}{f\sigma_r\sigma_t\sqrt{\sigma_t(3\sigma_r + 1.5\sigma_t)}} \quad (7)$$

We can evaluate these expressions if we make further assumptions about the beam size. For this purpose we have assumed an average beam size corresponding to two times the cathode radius. We find empirically that typical cathode radii scale with $1/\sqrt{f}$ for some operating machines. Longitudinally, we assume an average beam length corresponding to 10° fwhm of the rf. We make one further assumption: that the initial cavity has a geometry corresponding to that of AFEL in which $E_p = 1.56 E_{max}$. Figure 7 shows the peak surface field, E_p , as a function of frequency corresponding to optimum designs based on Kim's model. Also plotted for reference are one and two times the Kilpatrick sparking criteria and some actual values for operating machines.

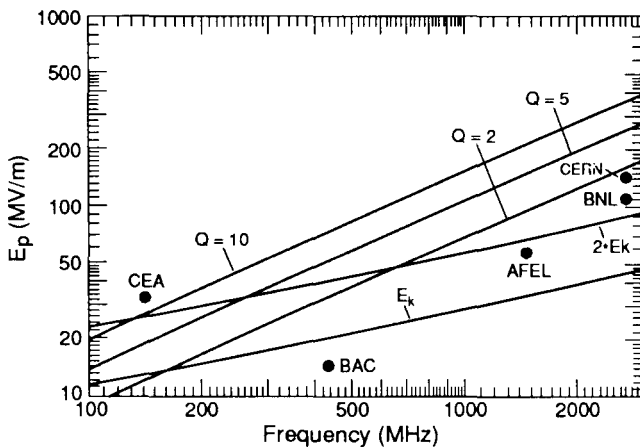


Fig. 7 Peak surface field vs. frequency for optimum photoinjector designs.

Figure 8 shows the expected emittance corresponding to the same optimum design criteria. The actual values for operating machines are again plotted for reference. While the model is useful in understanding the design space, the slope of these curves is very sensitive to the beam sizes assumed, and care must be taken in drawing global conclusions.

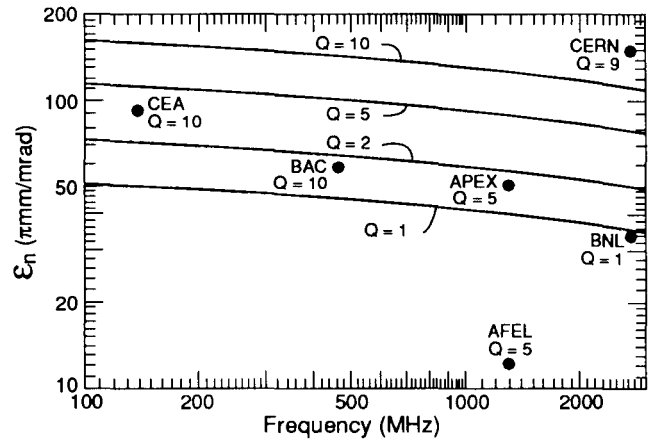


Fig. 8 ϵ_n vs. frequency for optimum photoinjector designs.

Emittance Control

The initial beam evolving from the surface of a photocathode is typically only tens of microns in length, resulting in extremely high charge densities. As space-charge forces begin to blow up the beam, the center of the bunch experiences larger forces than the head and tail. The resulting divergence creates a "bow-tie" in the phase space projection which is strongly correlated with longitudinal position. Carlsten has developed a space charge emittance compensation technique [5] which takes advantage of this correlation to recover most of the initial emittance.

By use of an external lens the beam emittance can be reduced simultaneously with focusing of the beam envelope. The lens alters the electron trajectories so that the space-charge forces acting on the beam after the lens cancel the effects of space-charge forces preceding the lens. As a result the bow tie can be made to vanish at the beam waist.

In practice we use a strong solenoid lens around the initial cells to implement Carlsten's scheme. The magnetic center of the solenoid lens is positioned so that electrons spend approximately as much time ahead of the lens as they do behind it. The strength of the solenoid is adjusted to create a minimum in the emittance at the entrance to the wiggler magnet.

Care must be taken not to allow magnetic field lines to penetrate the cathode itself. Electrons born in the solenoid field will have residual angular momentum as they emerge from the lens, causing in a hole in the emittance. The magnet configuration and resulting field shape for AFEL are shown in Fig. 9. Note that a separate bucking magnet, excited in the reverse direction, is used to "push" the field lines off the cathode. This technique provides considerable enhancement to the optimum performance that might be expected from Kim's model, which does not include any external restoring forces.

This technique should have general applicability but may be difficult to implement in very low frequency structures. It is likewise difficult to implement in 3-GHz photoinjectors of present design because of mechanical interference with the waveguide. All but the 3-GHz designs plotted in Fig. 8 use some degree of solenoid focusing, which accounts for their performance exceeding the model prediction.

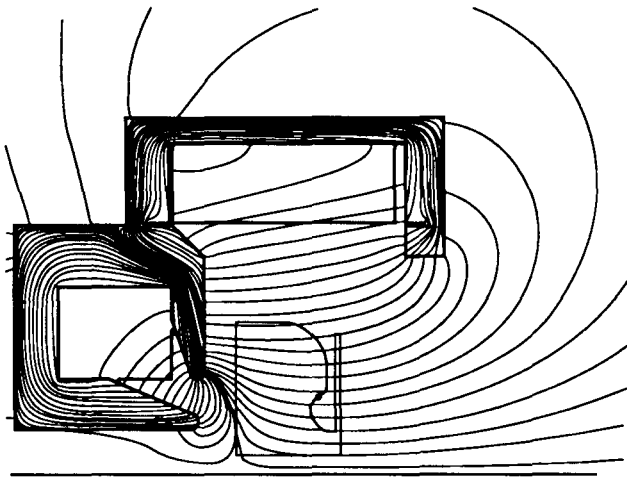


Fig. 9 AFEL solenoid magnet.

Field Emission

In practice, field emission has become a potential problem for high duty factor machines. Even without laser illumination the cathode can put a few microamperes of electrons into every rf bucket. The resulting charge in the accelerated "dark current" during an rf macropulse can equal the charge in the micropulse of interest.

Field emission is not well understood but is known to be related to the peak field on the surface of the cathode, the work function of the emitter, and the texture of the cathode. Dark current has been essentially eliminated in AFEL by polishing the cathode substrate. This has not solved the problem at higher frequencies where there are very high fields on the cathode. Field emission may well be the limiting factor in the design of high frequency high gradient photoinjectors.

Conclusion

We have reviewed a small subset of the design parameter space for photoinjectors and it would be presumptuous to draw any global conclusions. We can, however, make some observations. A practical photoinjector design optimized for

high-duty FEL applications would be L-band so that the structure could be effectively cooled and it could accommodate a practical solenoid. It would operate at a modest electric field gradient to increase reliability, minimize sparking, reduce power dissipation, and control field emission. It would incorporate solenoid focusing to control space-charge induced emittance growth. Actually the design of many existing photoinjectors is very mature in these areas and future work in the field will probably concentrate on increasing cathode efficiency and simplifying the drive lasers.

Acknowledgements

The author thanks Bruce Carlsten and Patrick O'Shea for tutoring him in the theoretical and practical aspects of the art and Lloyd Young and Jim Billen for generating the figures for this paper and for many enlightening discussions.

References

- [1] R. L. Sheffield et al, "RF Photoelectron Gun Experimental Performance," Proc. 1988 Linear Acc. Conf., CEBAF Report-89-001, June 1989, p. 520.
- [2] L. Serafini et al., "TOPGUG: A New way to Increase the Beam Brightness of RF Guns," INFN/TC-91/07 (1991).
- [3] L. Serafini et al., "Numerical Simulations for the ARES Superconducting Low Emittance Injector," INFN/TC-90/10 (1990).
- [4] K. J. Kim, "RF and Space-Charge Effects in Laser-Driven RF Electron Guns," NIM, A275, 1989, p 201.
- [5] B. E. Carlsten, "New Photoelectric Injector Design for the Los Alamos National Laboratory XUV FEL Accelerator," Nucl. Instr. and Methods in Physics Res. A285,313 (1989).